Engineering Structures 202 (2020) 109853

Contents lists available at ScienceDirect

Engineering Structures

journal homepage: www.elsevier.com/locate/engstruct

Predicting residual deformations in a reinforced concrete building structure after a fire event

Shuna Ni, Thomas Gernay*

Dept. of Civil Engineering, Johns Hopkins University, Baltimore, MD 21218, United States

ARTICLE INFO

Keywords:
Fire
Reinforced concrete structures
Numerical modeling
Residual deformations
Resilience

ABSTRACT

Reinforced concrete (RC) structures often remain stable under fire, but exhibit damage and residual deformations which require repairs. While repair operations and building downtime are expensive, current fire design approaches do not consider post-event resilience. The first step to enable predicting the resilience of RC structures under fire is to develop capabilities to model the damage of these structures after various fire exposures. This paper focuses on the prediction of the residual (post-fire) deformations of RC columns within a code-designed five-story RC frame building. Computational modeling approaches to capture the fire behavior of the columns are investigated. The models range from isolated columns with linear springs at the boundaries to full building model coupling beam and shell elements, with intermediate approaches. The analyses highlight the critical nonlinear role of the thermal expansion-contraction of the surrounding beams and slabs on the column deformations. Large transversal residual deformations develop particularly in perimeter columns, combined with residual shortening. This invalidates models based on isolated column or 2D frame. A parametric study of the residual deformations of RC columns is then conducted, with due consideration of the 3D restraints and interactions, to investigate the effects of different design parameters and fire scenarios on the residual deformations after a fire event. The results of the parametric study indicate that fire load density and opening factor significantly influence the residual deformations of RC columns, compared to the thermal conductivity of concrete and live loads. This research improves the understanding and provides recommendations for numerical modeling of the effect of fire on the residual capacity and deformations in RC structures.

1. Introduction

Reinforced concrete (RC) buildings generally exhibit a good structural performance under accidental fire events, as seen in, for instance, the 2005 Windsor Tower fire or the 2017 Grenfell Tower fire. In the two latter events, no global structural collapse of the concrete structure occurred, despite fires raging for hours. Yet, while fire does often not result in global collapse of RC structures, the potential loss due to downtime and repairs may be significant. In many instances, the fire accident is not as severe as in the two aforementioned cases, and a rehabilitation is possible [1,2]. The question of post-fire damage and downtime cost has gained increasing attention due to the requirements for resilience of structures under hazards. To develop optimum provisions to design fire resilient structures, engineers need the ability to accurately estimate the potential economic loss for different design alternatives due to fire damage. This in turn requires the ability to predict the behavior of RC structures under fire, including the residual deformations and residual load-bearing capacity of a structure after fire.

Structural members are often tested as independent elements under fire, disregarding global behavior. However, the proper inclusion of structural continuity of fire induced effects is crucial for an accurate evaluation of RC building's response. The heating of structural members leads to thermal expansion, which may cause the surrounding structure to impose high restraint forces. The significant impact of boundary conditions on the fire behavior of RC structures under fire has been observed in many historical accidents and previous research. In the Katrantzos Department Store fire (an eight-story RC building) in Greece in 1980, the restraints from differential thermal expansion in the structure led to the collapse of a major part of the 5th to 8th floors and the failures of various other floors and columns throughout the building [3].

Extensive research works have demonstrated the considerable effect of restraints on the behavior of RC structural members under fire, based on numerical or experimental studies of RC columns, beams, slabs and walls [4–11]. Therefore, proper modeling of these boundary restraint

* Corresponding author.
E-mail addresses: sni5@jhu.edu (S. Ni), tgernay@jhu.edu (T. Gernay).

https://doi.org/10.1016/j.engstruct.2019.109853
Received 23 May 2019; Received in revised form 14 September 2019; Accepted 22 October 2019

effects is essential when analyzing RC structures under fire.

However, previous numerical studies mostly adopted simple methods to simulate the restraint stiffness of structural components under fire, i.e. modeling isolated structural members under idealized boundary conditions. Those idealized conditions do not consider the variation of the surrounding restraints with fire, which stems from the change of restraint stiffness due to temperature degradation of the properties, as well as from the thermal expansion-contraction of the surrounding restraints [4]. Although some of the existing research has recognized the great deformation of the surrounding restraints, they have simplified the deformation of the surrounding structural members to an extent which even ignored the influence of critical structural components, for example, the sideway of a column under fire without considering the effect of the thermal expansion of slab [12]. Therefore, more research is required to propose a sophisticated yet computationally reasonable method to model the boundary conditions of a column part of a structure under fire.

Besides, previous research focused mostly on the heating phase for studying the effect of the surrounding restraints on the fire resistance of RC structural members, rather than investigating the post-fire residual deformations after heating-cooling. The structural behavior of concrete members is affected by both heating and cooling; severe damage may develop between the end of the heating phase and the full burnout, potentially leading to delayed failure [13]. To improve the resilience of RC structure under fire and minimize the economic loss from the fire damage of RC structures, the residual deformations of RC structural members after burnout should be accurately predicted.

Moreover, the concrete models used in existing research generally incorporate the effect of transient creep strain in an implicit manner. This does not allow capturing the effect on concrete behavior of the stress-temperature path nor the non-reversibility of the transient creep strain when the stress and/or the temperature is decreasing. While this limitation may be acceptable under heating, it is not appropriate under cooling and may lead to severe underestimating of residual deformations of a structural component after fire exposure [14–16].

To advance research on these issues, this paper focuses on the modeling of the residual deformations of RC structures after fire. The objective is to address some identified shortcomings with respect to the modeling of the effects of thermal expansion in structural assemblies as well as the effects of heating-cooling sequences and residual behavior, while accounting for sophisticated material models considering explicitly the transient creep strains. The fire behavior of a code-designed five-story RC frame is investigated. Numerical analysis by the finite element method (FEM) is adopted using SAFIR [17]. The main focus is on the behavior of the RC columns, while capturing the effects of interactions with the rest of the structure throughout the fire event. The behavior of RC columns as part of the full building model is compared to that of isolated columns under idealized boundary conditions. To reduce the computational cost, two intermediate modeling methods are introduced, where the structure surrounding the fire compartment is simplified. Those two methods aim to model the sophisticated boundaries of a column, notably the thermal expansion-contraction and the nonlinear response of the surrounding beams and slabs, while reducing the computational time with respect to the full building model. Results based on the intermediate models are compared to those from the full building model and the isolated column model. Then, parametric studies of the residual deformation of RC columns are conducted. These studies adopt the validated intermediate model. The parametric studies focus on four critical parameters, including fire load density, opening factors, thermal conductivity of concrete and live loads.

2. Prototype (code-designed) RC building

2.1. Description of the building

A five-story RC building was adopted as a prototype. The frame building consists of moment resisting frames in both orthogonal directions with 5 bays in each direction, having a 7.0 m span length, resulting in a 35 m by 35 m square floor plan (Fig. 1). A story height of 4.0 m was used for each floor including the ground level. The building was designed based on the 2010 NBCC seismic requirements with accompanying CAS Standard A23.3-04 “Design of Concrete Structures” used for proportioning and detailing of members [18–20]. The building is located in Vancouver and designed for residential or office occupancy with an importance factor of $I_E = 1.0$ (I_E is a function of risk category which is used to increase the margin of safety of a structure against collapse under earthquake [19]), on firm soil (Soil Class C). The design dead load included a superimposed dead load of 1.33 kPa consisting of floor finish, partition walls and mechanical/electrical fixtures, in addition to member self-weight. The live load was 2.4 kPa. It is designed to be a fully ductile frame, with $R_d = 4.0$ and $R_o = 1.7$ (R_d is the ductility-related modification factor reflecting the capability of a structure to dissipate energy through reversed cyclic inelastic behavior while R_o is an overstrength-related force modification factor accounting for the dependable portion of reserve strength in a structure designed according to the codes [19]). The characteristic compressive strength of concrete is 30 MPa and the characteristic yield strength of rebar is 400 MPa. Table 1 provides the design details for each member. The slab, designed according to CAS Standard A23.3-04 [20], is 200 mm in thickness, with two layers of reinforcement. The reinforcement ratio of the slab is adjusted in different regions based on ambient temperature design and according to construction practice.

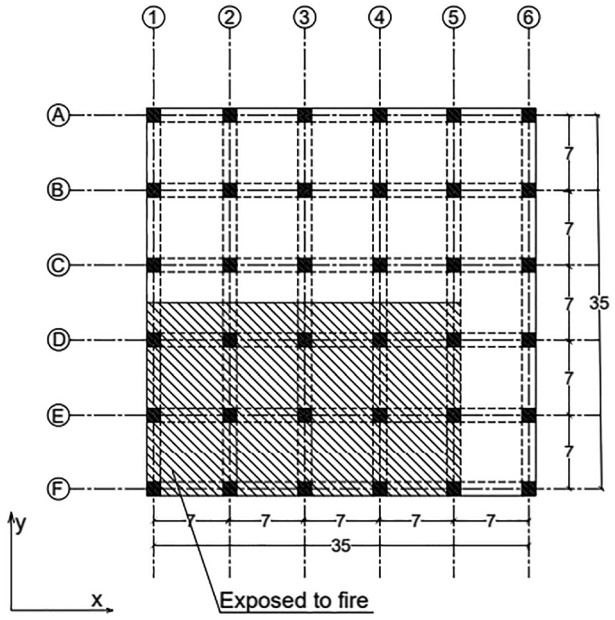

Fig. 1. Floor plan and region exposed to fire.

The building was designed for seismic loading [18], but no information was provided for the fire resistance of this building.

Table 1
Dimension of structural members.

		Size (mm × mm)	Steel reinforcement
Column	Corner Column 1–5	300 × 300	8–20 M
	Ext Column 1–2	300 × 300	4–30 M
	Ext Column 3–5	300 × 300	4–25 M
	Int Column 1–2	450 × 450	12–25 M
	Int Column 3–5	450 × 450	4–25 M + 4–20 M
Beam	Ext Beam	300 × 500	Top: 3–20 M Bottom: 2–20 M
	Int Beam	300 × 500	Top: 3–25 M Bottom: 2–25 M

Table 2
Summary of the parameters in the thermal-mechanical analysis.

Fire analysis		
Fire load density		640, 480 and 320 MJ/m^2
Opening factors		0.035 m$^{1/2}$
ta[(1)]		300 s
Fire grow rate		Medium
Thermal inertia of boundary		1400 J/m^2 s$^{1/2}$ K
Thermal analysis		
Film coefficient on hot surface		35 W/m^2 K
Film coefficient on cold surface		4 W/m^2 K
Emissivity		0.7
Parameter for thermal conductivity of concrete [(2)]		0.5
Specific heat of concrete at 20 °C		900 J/kg K
Density of concrete		2300 kg/m^3
Water content		46 kg/m^3
Mechanical analysis		
Additional dead load		1.33 kPa
Live load		2.40 kPa
Snow load		3.02 kPa
Concrete model	$f_{c,0}$	30 MPa
	$f_{t,0}$	1 MPa
	ν_c	0.2
	$\varepsilon_{c1,0}$	0.0025
	α_g	0.25
	x_c	0.19
	$\tilde{d}_c$	0.3
	g_t	2000 N/m^2
Steel model	**Type of steel**	Hot rolled, Class B
	$f_{y,0}$	400 MPa
	ν_s	0.3
	E_s	200 GPa

Note: (1) ta is the time needed to reach a rate of heat release of 1 MW [22]; (2) The thermal conductivity can be chosen between a lower and upper limit value [25]. The parameter α allows any intermediate value to be taken, with α = 1 being the upper limit and α = 0 being the lower limit; linear interpolation is used in between.

According to the occupancy type of this building, the fire ratings of the structural members are designed for a Type II A construction as per the IBC [21]. The fire separation distance from other building is greater than 30ft. Therefore, the fire resistance rating requirements for the primary structural frame is one hour, one hour for floor construction and associated secondary members and one hour for roof construction and associated secondary members. No requirements are specified for exterior and interior partition walls. The concrete cover thickness for the primary members and slab meet the fire resistance requirements. The interior partition wall is a one-hour fire-resistance STC57 walls and the exterior wall system is a frame wall with exterior rigid insulation with cavity insulation and stucco.

2.2. Modeling of the building in SAFIR

The nonlinear finite-element software SAFIR [17] is used to conduct the heat transfer analysis in the structure, followed by the transient structural analysis. The reference fire scenario is based on a fire developing over a 28 m by 17.5 m area on the ground floor, as shown in Fig. 1. The parameters adopted for the reference fire scenario are shown in Table 2. Three different design fire load densities are selected: 320 MJ/m^2, 480 MJ/m^2 and 640 MJ/m^2. Those values are obtained by multiplying fire load densities of 400 MJ/m^2, 600 MJ/m^2 and 800 MJ/m^2 by a combustion factor of 0.8. The latter fire load densities range from average to severe values for office occupancy based on statistical data. The fire growth rate is taken as medium (ta equal to 300 s) according to the Eurocode 1 (2002) for an office building [22]. The opening factors are selected based on an assumption of the openings' layout and number of windows and doors which are broken during the fire. The effect of this parameter will be investigated in the parametric

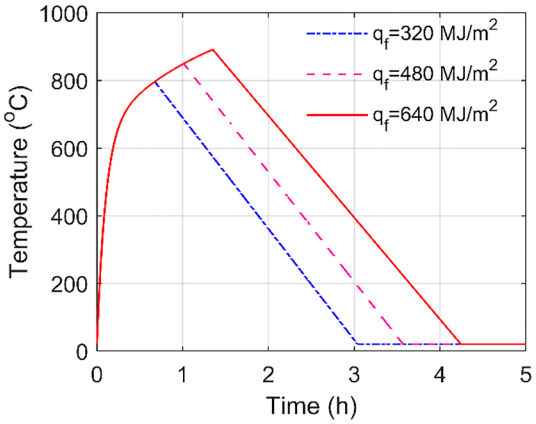

Fig. 2. Gas temperature-time curves.

analysis. The thermal inertia of boundary enclosure is selected based on the assumed materials lining the fire compartment (concrete ceiling, concrete floor, interior STC57 wall and exterior frame wall with exterior rigid insulation with cavity insulation and stucco). The parametric fire model in the Eurocode 1 (2002) [22] is used to calculate the gas temperature. The gas temperature–time curves in the compartment are shown in Fig. 2.

In the mechanical analysis, the columns and beams are modelled using beam elements while the slab is modelled using shell elements, shown in Fig. 3. The material models for beam elements are SILCON_ETC and STEELEC2EN while the material models for shell elements are SILCOETC2D and STEELEC2EN. The concrete models are described in detail in former publications [23,24]. The concrete model for shell is based on a plasticity-damage formulation. As mentioned in Section 1, the ETC models (SILCON_ETC and SILCOETC2D) incorporate the transient creep strain explicitly. The temperature dependency of the properties of those models is in accordance with the recommendations of EN 1992-1-2 Table 3.1, Table 3.2 and Figure 3.2 [25]. The STEELEC2EN model is the uniaxial law for steel from the EN 1993-1-2 [26]. Perfect bond between steel reinforcement and concrete is assumed in the analysis.

The inputs for the concrete and steel models are listed in Table 2. For concrete, the inputs include compressive ($f_{c,0}$) and tensile ($f_{t,0}$) strength at ambient temperature, Poisson's ratio (ν_c), strain at peak stress at ambient temperature ($\varepsilon_{c1,0}$), dilatancy parameter (α_g), compressive ductility parameter (x_c), compressive damage at peak stress ($\tilde{d}_c$), and tensile ductility parameter (g_t). Recommended values are given in [23] and adopted here. The tensile ductility parameter is the

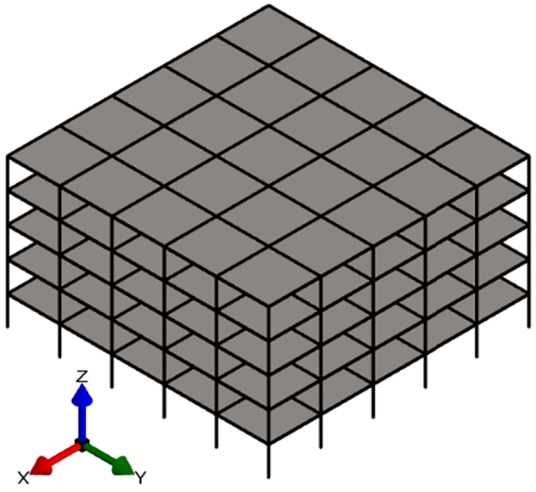

Fig. 3. SAFIR model of the building.

regularized tensile fracture energy (in N/m^2) which is defined as the ratio of the fracture energy (in Nm/m^2) to a characteristic length (in m) [23]. The value adopted for tensile ductility parameter accounts for tension-stiffening due to the presence of the reinforcement. The adopted value of 2000 N/m^2 is thus greater than for plain concrete, but it corresponds to the lower bound of the tension-stiffening behavior of reinforced concrete recommended by several sources [27–30].

Spalling is not considered in this study. There is currently no available modeling approach to predict the occurrence of spalling at the scale of an entire structure. It must be noted that the building is made of normal strength concrete with low water content, and the fire event is assumed to occur in an existing (relatively old) building, which are factors contributing to lower the risk of spalling (although admittedly not eliminating it completely).

3. Benchmark for computational modeling of RC structures under fire with heating and cooling phases

3.1. Validation against fire tests on RC structures

This research relies on numerical modeling of the thermal-mechanical response of RC structures based on the finite element method. The main assumptions and modeling techniques adopted in the work have been detailed elsewhere; see notably [17] for the software, [31] for the shell finite element, [23] for the multiaxial concrete model. In terms of validation, while no full-scale fire test of a similar five-story RC building under this type of fire scenario has ever been performed, tests on elements and parts of structures have previously been modeled for benchmarking the numerical modeling approach.

A series of tests on axially restrained RC columns under heating and cooling [6] have been simulated using SAFIR in prior works [15]. The columns were axially restrained using a restraining beam, shown in Fig. 4a. The columns were initially concentrically loaded and then subjected to the standard ISO fire on the four sides; finally, they were allowed to cool down while still under loading. Two different levels of axial restraint and loads and two types of geometries of cross-section were considered, leading to eight different cases. The particular interest of these tests laid in the facts that the RC columns were restrained and that the response was measured during the cooling phase as well, hence including the residual value of the axial shortening. Results show that the numerical model captured the experimental behavior throughout the entire fire duration, see Fig. 4b. Explicit modeling of transient creep strain was key for following the experimental response during cooling [15].

Another relevant benchmark, previously published, is the full-scale FICEB fire test. This test dealt with a loaded steel-concrete composite floor supported by cellular beams and subjected to a natural wood crib fire. Details of the test are presented by Vassart et al. [32], while the SAFIR numerical model has been described by Gernay and Franssen [33]. The numerical model was able to predict not only the tensile membrane action of the composite slab under fire but also the residual deformations of the structure after fire exposure. It is worth noting that the test was numerically simulated with SAFIR before being conducted, to help with design and prediction of the behavior. This blind prediction provided good results, capturing the qualitative behavior in tensile membrane action and predicting no failure. Different methods of accounting for instability of the central cellular beams led to predicted displacements that bounded the test results. After the test, the simulation was repeated with adjustment of the fire load (which had eventually been increased in the test versus what was planned) and a modified steel model for capturing the effect of web post buckling; this post-test simulation provided maximum vertical deflections at mid-span of the central beam within 8% of the measurements [17]. Although the tested floor was a steel-concrete composite floor, it provides a useful benchmark in terms of validation of the ability to capture the damage and permanent deformations in RC slabs subjected to fire.

A third benchmark against test data is presented in the next section, where the issue of mesh sensitivity is also discussed.

3.2. Mesh sensitivity analysis for a slab in tensile membrane action

The RC slab noted as HD 12 in Lim's tests report [34] has been modeled with SAFIR. For this test, a loaded RC flat slab of dimensions 3.3 m × 4.3 m was subjected to ISO fire for 3 h. The slab developed tensile membrane action and survived the fire exposure.

As the computation efficiency of a full building model is notably influenced by the number of shell elements used for the slabs in the model, it is important to study the required mesh density for the slab under fire. Therefore, a mesh sensitivity analysis was conducted on the numerical model. The objective was to verify convergence of the numerical solution to the "true" solution (assuming the solution obtained with a fine mesh is the true solution). It is noteworthy that the case study involves concrete in tension, which is known to be a potential source of mesh sensitivity due to softening. Three different mesh sizes were investigated: Mesh 11 × 11, Mesh 16 × 16 and Mesh 21 × 21 (the number indicates the number of elements along the x and y dimensions of the slab model, which comprises one quarter of the full tested slab owing to symmetry). Fig. 5a compares the test and simulation data in terms of vertical deflection at the center of the slab. No mesh sensitivity was observed in the numerical analysis of the RC slabs.

Since this paper focuses on the residual deformation of RC structural members after fire exposure, in addition to the ISO fire in the test,

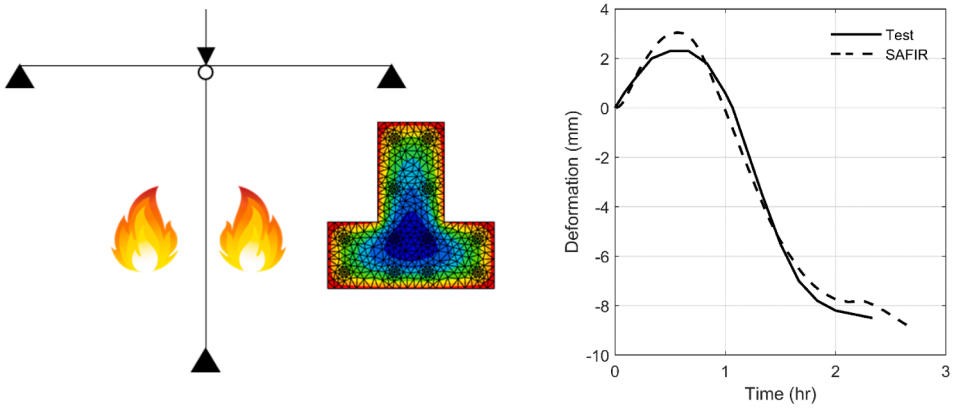

(a) Test setup and column section (b) Axial deformation under fire

Fig. 4. Benchmark of the numerical model against test data on restrained RC columns subjected to heating and cooling, shown here for column RCT 21 in Wu's test [4], with more results published in [15]. The displacements are accurately captured, including the residual axial deformation.

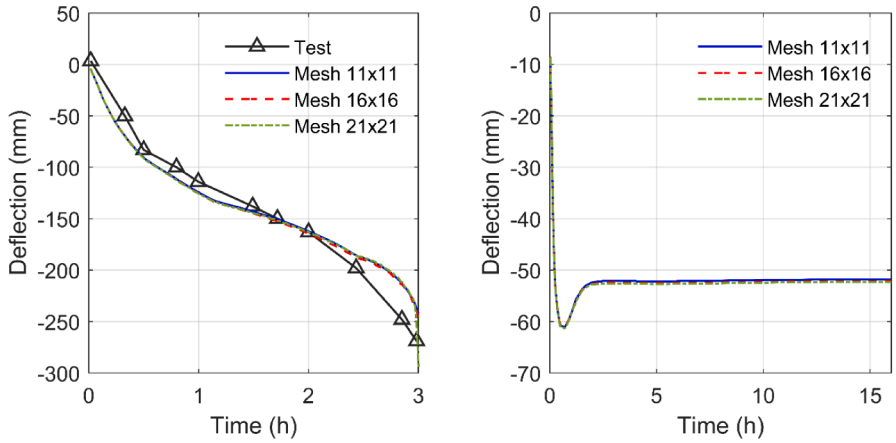

(a) Under ISO fire, including comparison to test data

(b) Under a heat-cooling fire scenario (not performed experimentally)

Fig. 5. Numerical analysis of a loaded RC slab under fire: comparison with experiment and mesh sensitivity.

another fire scenario with cooling phase is considered (Fig. 5b). For this scenario, no test data is available. The comparison of numerical results from models of different mesh sizes indicate that the residual deformation of RC slab with membrane action is not sensitive to mesh size. Accordingly, a reasonably efficient mesh size can be selected for the modeling of slab in the full building model.

In the model, the tension behavior uses a regularized tensile fracture energy to handle the softening behavior. The regularized tensile fracture energy (in N/m^2) is defined as the ratio of the fracture energy (in Nm/m^2) to a characteristic length (in m) [23], as discussed in Section 2.2. The characteristic length is used to define a representative dimension of the mesh size in which it is assumed that the fracture energy is uniformly dissipated when a single crack is assumed to localize in a single finite element. When a slab develops tensile membrane action, it experiences a relatively uniform tensile cracking over the entire slab, instead of a localized (single crack) failure. Besides as the slab is reinforced with a steel mesh, the tension is carried by the steel reinforcement and tension-stiffening develops. This might explain why the slab behavior is not mesh-dependent [35], and a constant value of the regularized tensile fracture energy is used between the different numerical analyses for the concrete incorporating the tension-stiffening effect ($g_t = 5000\,N/m^2$). As the floors of the building under consideration are reinforced and will exhibit a similar behavior under fire, the same observation should hold, and the results of the columns deformations are not expected to depend significantly on the slab mesh size.

3.3. Additional considerations when modeling the residual response of RC members

3.3.1. Transient creep strain of concrete

A major component to take into account in fire-exposed concrete is the transient creep strain which develops during first-time heating of concrete under stress [36,37]. Transient creep strain originates in the irrecoverable damage of the cement paste. It noticeably affects the behavior of fire-exposed concrete structures. While there is a consensus regarding the need to include transient creep in any concrete model used for analysis of concrete structures in fire, two distinct modeling approaches remain in use, namely an implicit and an explicit one. Compared to explicit approach, the implicit approach is simpler but is unable to capture the effect of the stress-temperature path and the irreversibility of the transient creep strain when the stress and/or the temperature is decreasing [38]. This considerable drawback with the implicit approach potentially leads to unsafe predictions in particular (but not only) when modeling concrete structures under natural fires [15]. The ETC concrete model in SAFIR, which explicitly evaluates transient creep strain throughout the analysis, has been used in this research. This model is described in former references including validation against test data at the material and structural levels [38].

3.3.2. Residual thermal expansion of concrete

In regard to thermal elongation, test data indicate that concrete that is heated and then cooled down exhibits a residual thermal strain, the value of which is a function of the maximum reached temperature. A residual shrinkage has been reported after temperatures up to 400 °C, whereas a residual thermal expansion has been reported after temperatures of 600 °C and higher [24,39]. The adopted concrete models account for the residual thermal expansion of concrete, as described in [13] (the simulations in the present paper use the residual thermal model of Table 3 in [13]).

3.3.3. Residual properties of concrete

The properties of concrete are known to be permanently affected by heating. An extensive analysis of results from literature shows that the compressive strength of concrete will decrease further due to the further cracking during the cooling phase. Eurocode 4 (1995) [40] proposes an additional decrease of 10% from the high-temperature compression strength. This 10% additional compression strength reduction during cooling is accounted for in the software SAFIR. The residual tensile strength is kept at the value corresponding to the maximum reached temperature.

3.3.4. Residual properties of reinforcement

Existing research about the residual mechanical properties of steel reinforcement after exposure to high temperature is limited and exhibits scatter, but tends to indicate that yield strength of common grade steel reinforcement is recovered to initial value during cooling if the temperature has not exceeded (at least) 600 °C [41–44]. Beyond this

Table 3
Effect of fire on the maximum applied load (at last converged time step) on the building (fire scenario with 640 MJ/m^2).

	Increase all loads to failure	Increase point loads to failure
No fire (kN)	130 893	179 984
After fire (kN)	57 307	57 254
Percentage decrease (%)	56.2	68.2

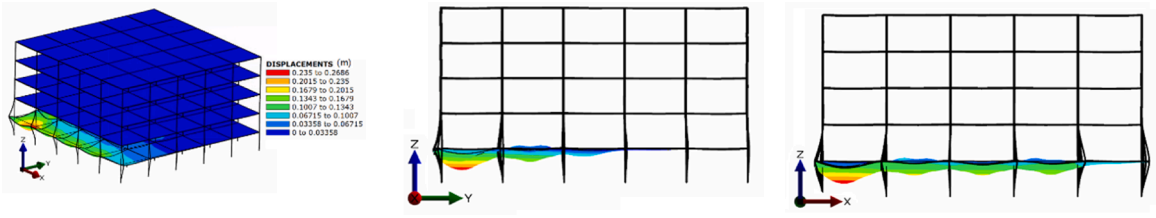

Fig. 6. Deformation of the building during the fire scenario with $q_f = 640\ MJ/m^2$.

temperature of 600 °C, assuming some degree of permanent loss of yield strength for each degree exceeding the threshold seems justified, but more data is required. Steel models in SAFIR allow inputting the degree of loss of residual strength of reinforcement. Steel thermal properties are generally considered as reversible. In the numerical analysis below, both the thermal and mechanical properties are assumed to be reversible.

4. Behavior of the prototype building under fire

4.1. Overall fire behavior of the building

The FE model described in Section 2.2 is run under the fire based on a fuel load density of 640 MJ/m^2 (shown in Fig. 2). The heating phase of the fire scenario lasts for 81 min followed by a cooling phase. However, due to the high thermal inertia of the structural members, the temperature continues to increase in the sections long beyond 81 min. Fig. 6 shows the deformation of the building at 204 min when the thermal expansion of most structural members is maximum. Fig. 6a depicts the overall deformation of the building; Fig. 6b shows the front view of the building where the first two and a half bays from the left in the first story have been exposed to fire; Fig. 6c is the side view of the building where the first four bays from the left in the first story have been exposed to fire.

The residual deformation of the RC building after the fire event is shown in Fig. 7. The comparison of the maximum (shown in Fig. 6) and the residual deformation (shown in Fig. 7) of the building indicates that the building recovers some deformation during the cooling phase; however, the recovery is limited. Most fire-exposed structural members (slabs, beams and columns) have considerable residual deformations after the fire event. The structural members which are not directly exposed to fire may also have residual deformation, e.g., the right exterior column on first and second story in Fig. 7c. Structural members above the second story have negligible residual deformations. As a conclusion, the fire event lead to significant permanent deformations of the structural members at the level of the fire and those directly above, while the effect is limited for members at higher levels.

Fig. 8 shows the distribution of the residual mechanical strains in the top section of the column F2. Column F2 is a perimeter column which was exposed to fire directly on its sides 1, 2 and 4 (see Fig. 1 for column labels). The maximum compressive residual strain is 0.203 and

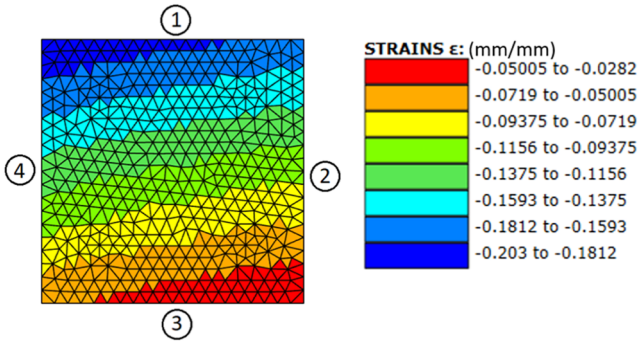

Fig. 8. Residual mechanical axial strain in the top section of the column F2.

the minimum compressive residual strain is 0.0282, which indicates that the whole section is in a state of compression beyond the elastic limit.

4.2. Fire behavior and residual deformations of the first-story columns

The maximum deformations of the columns during the fire and their residual deformations after fire are investigated. The scenario with fire load density of 640 MJ/m^2 is taken as an example. Fig. 9 shows the displacement color map of RC columns after the fire. The RC columns experienced considerable deformations in both axial (Z) and lateral (X and Y) directions during the fire; the recovery of those deformations is limited after the fire event.

The lateral deformations at the column tops are particularly significant, with maximum values exceeding 80 mm and residual values of the order of 50 mm in X or Y directions, in some cases. Compared to the perimeter columns size of 300 mm × 300 mm, these displacements are large. These are mostly due to the thermal expansion of the floor members (beams and slabs) in their plane. These floor members exert horizontal forces on the columns that generate permanent transversal deformations, as shown on the profiles of Figs. 6 and 7. The thermal gradients acting on the perimeter and corner columns also generate curvature, but the latter effect is minor compared to the displacements caused by the horizontal members. These aspects will be discussed further in the next section when considering isolated column models with springs. It will be shown that an important shortcoming of the

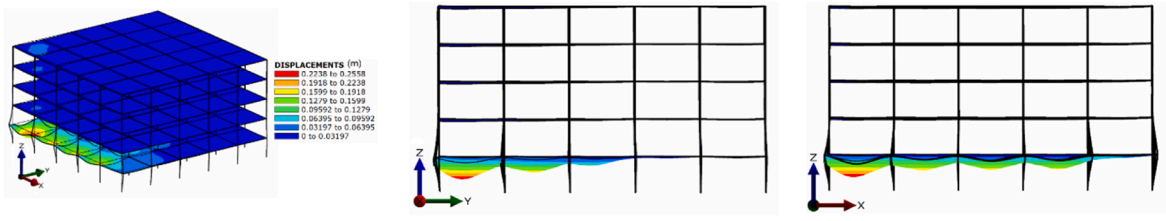

Fig. 7. Residual deformation of the building after the fire scenario with $q_f = 640\ MJ/m^2$.

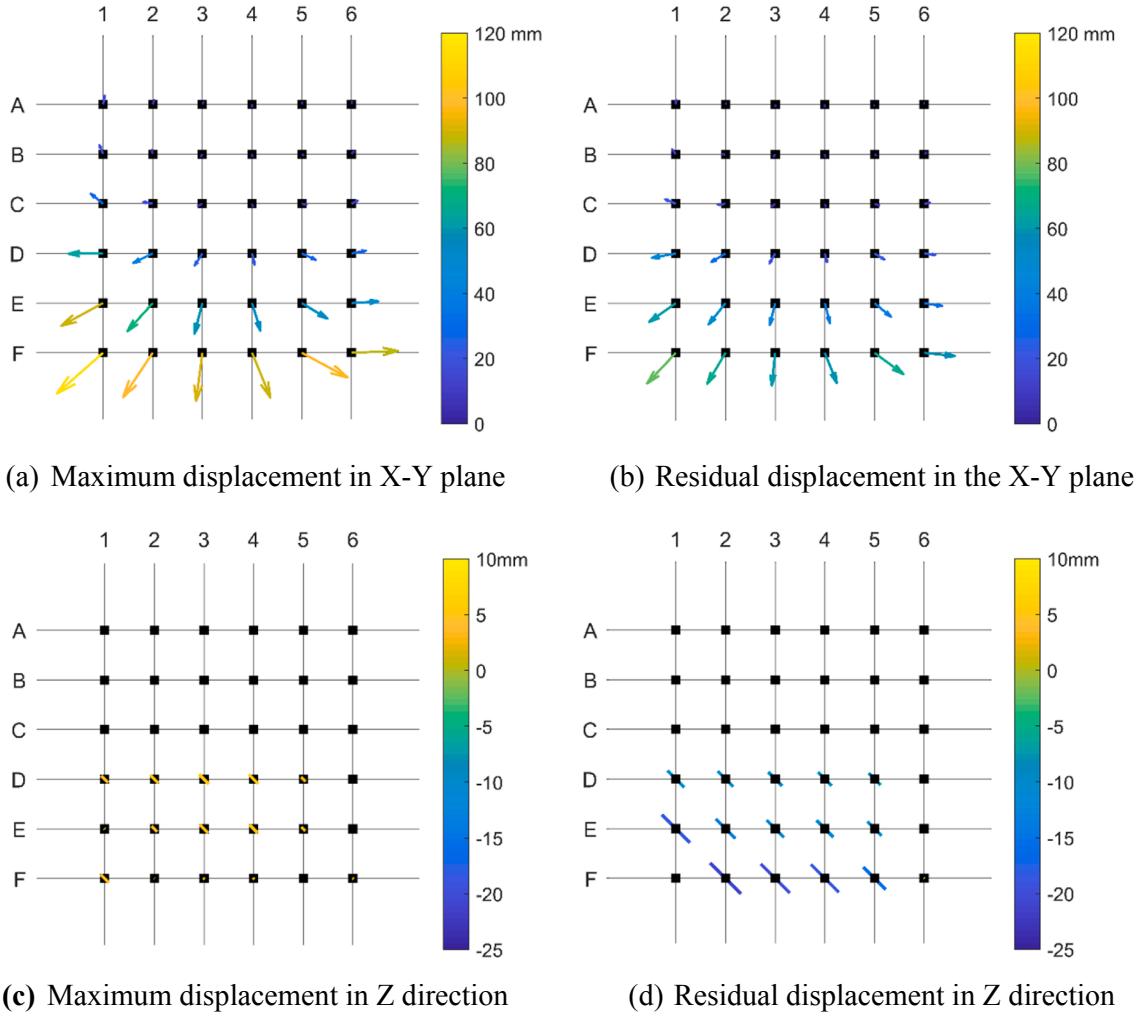

(a) Maximum displacement in X-Y plane (b) Residual displacement in the X-Y plane

(c) Maximum displacement in Z direction (d) Residual displacement in Z direction

Fig. 9. Colormap of maximum and residual column deflection under fire scenario with $q_f = 640\,MJ/m^2$ from full building model.

isolated column approach is the impossibility to capture the effects of thermal expansion-contraction of the fire-exposed floors, which are responsible for most of the permanent horizontal deformations.

The behavior of columns varies with their initial loads, as well as their mechanical and thermal boundary conditions. From Fig. 9, the corner column F1 (labelled on Fig. 10d) experiences the maximum lateral displacement during the fire and the maximum residual lateral displacement due to the accumulated thermal expansion of its surrounding structural members and its unsymmetrical fire exposure. However, the residual axial deformation of the corner column is not as considerable as other columns (such as the exterior column F2 and the interior column D3) due to its relatively low initial axial load ratio [45]. The displacement histories of the three columns at their top node are plotted in Fig. 10. The exterior column F2 experiences the most residual axial shortening due to its size being smaller than D3 while its load is higher than F1. Examination of the finite element results shows that crushing occurs at the top of the column F2, which results in the large residual axial displacement at that location.

4.3. Residual load bearing capacity

In this section, the building post-fire load-bearing capacity is compared to that of the building without fire damage. The scenario with fire load density of $640\,MJ/m^2$ is considered. Two different loading procedures are investigated. The first loading procedure is to increase all the gravity loads of the building uniformly (including dead loads, superimposed dead loads, live loads and snow loads) until failure of the building (defined as lack of convergence of the finite element analysis due to material failure). The second loading procedure is to apply axial gravity point loads to the column tops at the first story and increase these loads until failure of the building. The axial loads at different column tops increase proportionally to the axial force of those columns under the gravity loads at ambient temperature. The load-bearing capacity of the building is the sum of all the applied gravity forces at the end of the simulation.

First, the case where all the loads of the building increase uniformly is discussed (loading procedure 1). The failure of the building without fire damage initiates at the perimeter RC columns F3 and F2 at the first story; damage also appears in their surrounding structural members (beams and slabs). Fig. 11a shows the area of the structure where reinforcement steel yielding and concrete crushing occurred at the end of the numerical simulation, in red and yellow colors. The initial axial load ratio of the perimeter columns at the first story is similar to that of the interior columns (the former being smaller in size), ranging from 0.33 to 0.39; however, these perimeter columns are subjected to greater bending moment at the top compared to the interior columns. As the loads increases uniformly, failure eventually develops in the perimeter columns due to combination of axial load and bending moment. In case of post-fire loading, the failure concentrates in the same area, on the fire-damaged perimeter RC column F2 and the surrounding beams, slabs and upper-story columns, as shown in Fig. 11b. Those columns have experienced severe fire damage and have greater residual

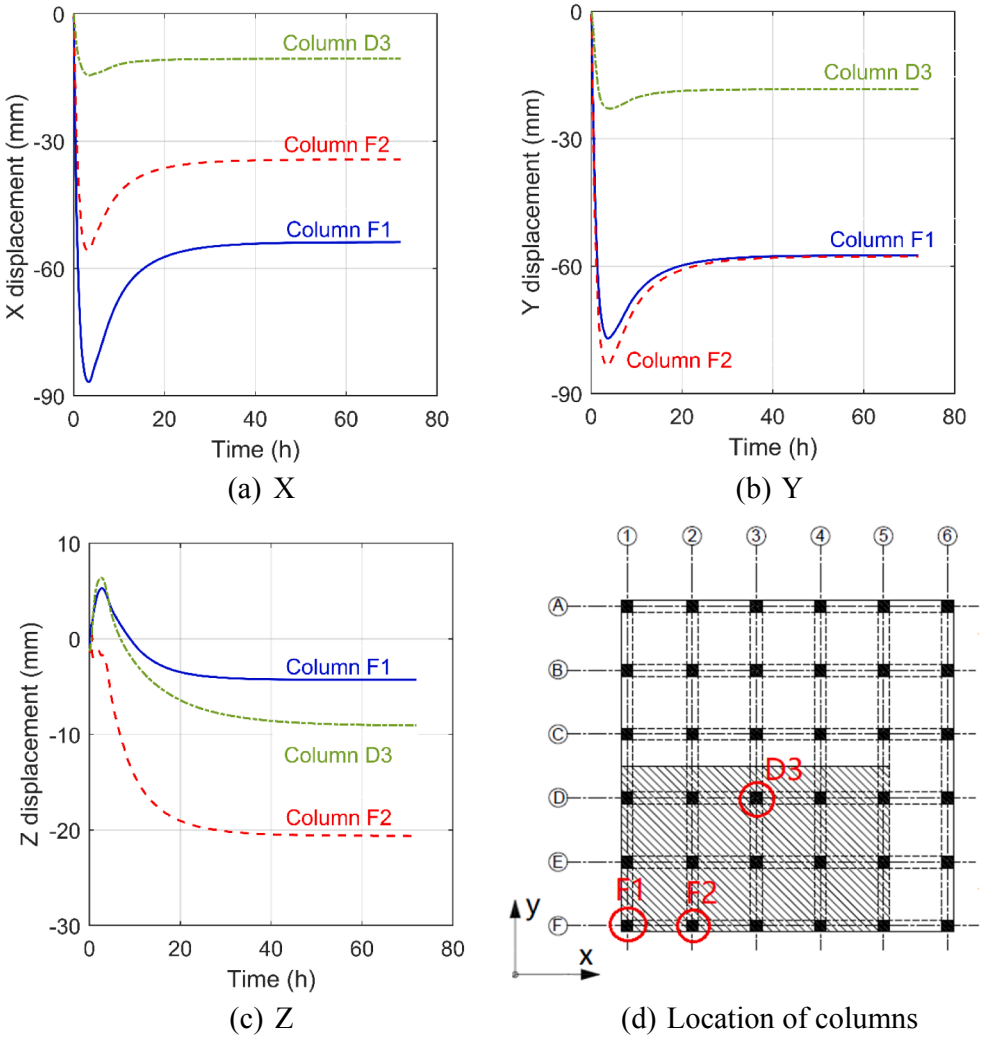

Fig. 10. Deformation of columns (column top) under the fire scenario with q_f = 640 MJ/m^2.

deformation, up to 67 mm in the X-Y plane, than interior ones. Although failure develops from the same area, the total gravity load supported by the post-fire building is 56% smaller than the maximum load supported by the undamaged building. Such considerable reduction in capacity may potentially nullify the safety factor used in the design of the building. Further analyses of the implications in terms of possible rehabilitation will be the subject of follow-up studies.

In the second loading procedure, the failure of the building without fire damage initiates at the interior column E2 at the first story, shown in Fig. 12a. Indeed, failure occurs first for the interior column which has the highest axial load ratio, because the bending moment on perimeter columns is not increased the same way it was in the first loading procedure. However, when looking at post-fire residual capacity, failure of the building initiates at the fire-damaged perimeter RC column F2 and then the damage extends to other fire-damaged exterior columns and their surrounding structural members, shown in Fig. 12b.

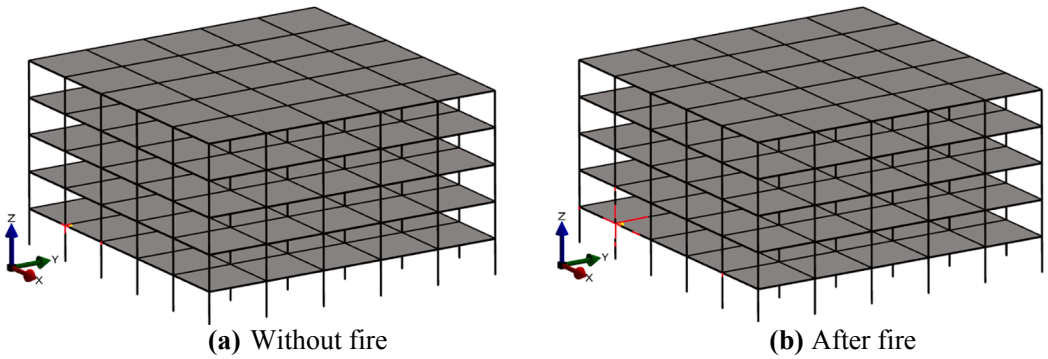

Fig. 11. Damage of the building as all the loads increases. Regions in red are the damaged beams or columns; regions in yellow are the damaged slabs. (For interpretation of the references to colour in this figure legend, the reader is referred to the web version of this article.)

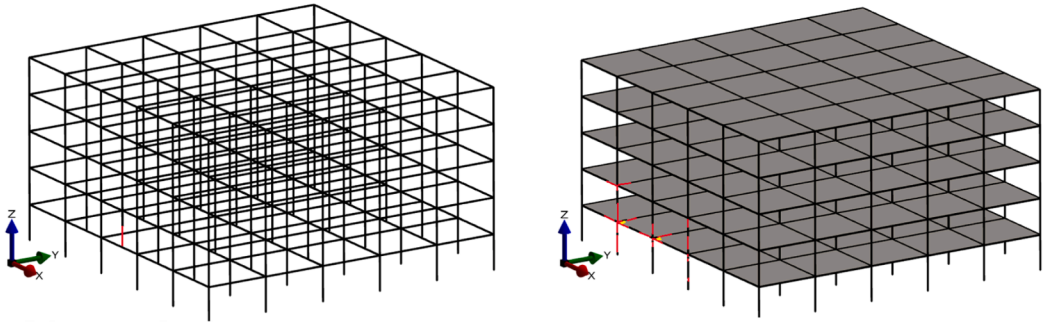

(a) Without fire **(b)** After fire

Fig. 12. Damage of the building as axial point loads increase proportionally at column tops. Shell elements have been removed in (a) in order to show the damage of the interior column E2. Regions in red are the damaged beams or columns; regions in yellow are the damaged slabs. (For interpretation of the references to colour in this figure legend, the reader is referred to the web version of this article.)

The loading procedure is found to influence the maximum applied gravity load for the building that it is not damaged by fire, with the second procedure leading to a higher load-bearing capacity. This is due to the fact that the increasing axial point loads (procedure 2) mainly magnifies the axial force of the columns while the uniform increase of all loads (procedure 1) magnifies both axial force and bending moments of the columns. However, for the post-fire building, the maximum applied load does not appear to depend on the loading procedure, and failure of the building under the two loading procedures develops in the same perimeter column area. According to Table 3, the residual load-bearing capacity of the building under both loading procedures is less than 50% of its original load-bearing capacity. This is a very significant reduction; much larger than what was observed for instance for the residual lateral load-bearing capacity of RC walls [46,47].

5. Computational model for a column part of a structure

The full building model discussed above is computationally expensive to run (computation time of the order of 18 h on 4 cores of Intel (R) Core (TM)i7-8700 CPU @3.2 GHz). In this research, the focus is on predicting the residual displacements in columns after a fire event. Therefore, some parts of the structure could be removed from the model to improve computational efficiency while maintaining accuracy in the columns' behavior prediction. Three different methods with different levels of simplification are discussed below: Isolated column model; one-story model; and simplified full building model.

5.1. Method 1: Isolated column model

Method 1 is commonly used in the literature [6,10,48] (see scheme reported in Fig. 13a). Translational elastic springs were used to model the translational restraint of the column top in lateral directions (X and Y directions) and axial direction (Z direction). An additional elastic beam element was added to the column top to model the rotational springs. The transfer of the bending moment and torsion between the elastic element and the column top is controlled by the rotational stiffnesses while the node at the other end of the additional element has its rotational degree of freedom fully restrained and is free in translational motion. The restraint stiffness of a target column along one degree of freedom (DoF) is determined by removing the target column from the full building model and imposing a unit displacement along that DoF at the location where the target column was originally attached while the other DoFs of that point are free to follow the rest structure, shown in Fig. 13b. The restraint stiffness is the force to have such as unit displacement. The restraint stiffnesses were determined for three of the building columns (corner column F1 exposed to two-side fire, exterior column F2 exposed to three-side fire and interior column D3 exposed to four-side fire). The stiffness values are given in Table 4 for the six degrees of freedom. The initial loads applied to the top of the isolated column model (shown in Fig. 13a) are calibrated to yield the same initial internal forces in the isolated column as those of the column in the full building model.

The fire scenario with fire load density of 640 MJ/m^2 is applied to the isolated column. The obtained residual deformations are compared to the results from the full building model in Table 5. It is clear that the isolated column model cannot predict accurately the residual deformations at the top of the column. Lateral deformations (X, Y) are drastically underestimated by the isolated column model. Axial deformations are accurately predicted for column D3, but not for column F2. This outcome stems from the limits of the isolated column model: (1) an isolated member model cannot consider the effects of the thermal expansion-contraction of the surrounding structural members, thus failing to predict deformations in X and Y directions as well as the coupling effect between lateral and axial deformations; (2) linear springs cannot model the nonlinear change of the boundary conditions (such as the accumulation of damage in the surrounding restraints

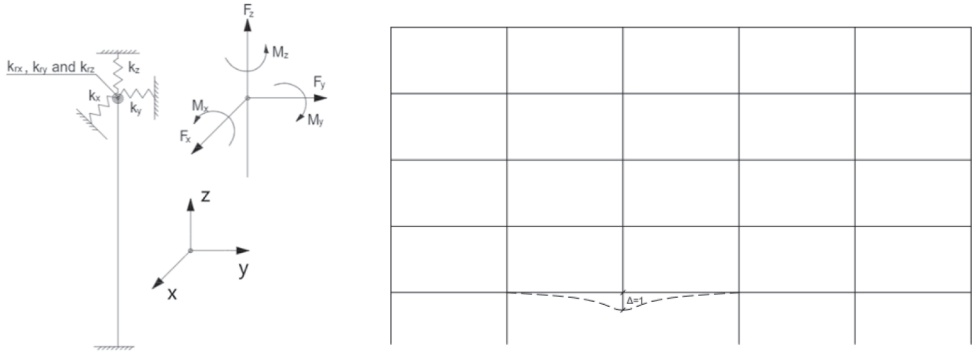

(a) Model **(b)** Calculation of restraint stiffness

Fig. 13. Isolated column model.

Table 4
Spring stiffness of the isolated column model.

	k_x (kN/m)	k_y (kN/m)	k_z (kN/m)	k_{rx} (kN·m/rad)	k_{ry} (kN·m/rad)	k_{rz} (kN·m/rad)
F1	47 795	47 795	30 270	73 295	73 295	14 830
F2	49 000	31 830	25 180	143 200	110 300	49 130
D3	73 020	73 020	107 400	283 450	283 450	63 040

under fire) and thus overlook the residual deformation contributed by the plastic deformation of the surrounding structural members; and (3) there is no consideration in the variation of the surrounding restraints with fire, which will lead to some errors when the surrounding structural members are also exposed to fire affecting their stiffness.

As the isolated column model is unable to capture the displacements in X and Y directions caused by the thermal deformation of the surrounding structural members, this method can only be used in fire scenarios where the surrounding members are not (significantly) heated. For instance, for a column exposed to localized fire, limited thermal force is exerted on the column from the expansion-contraction of the surrounding structural components, and the restraint stiffness remains relatively constant. Recent research has attempted to propose simplified equations to calculate the sideway of a column due to the thermal expansion of the surrounding structural members based on 2D models [12]. However, the latter only considers the thermal expansion of beams and ignores the effect from slab, which for the type of building under consideration will underestimate significantly the lateral deformations. Besides, the latter method does not consider the interaction between the thermal expansion in the X and Y directions.

5.2. Method 2: One-story model

To overcome the limitations of the isolated column model, another modelling method is introduced in this section. In this one-story model, the whole story where the fire develops is modelled, including the slab, beams and columns. Besides, the columns above the fire-exposed slab are also modelled, as shown in Fig. 14. The translational restraints (X, Y and Z) of the upper columns are modelled with linear springs. Since the upper stories are not exposed to fire, the rotations at the top of the upper columns are very limited and are thus neglected (assuming the rotations as completely restrained).

The stiffnesses of the springs at the top of the second story columns need to be calibrated. Calibration is done through a trial-error process to match the deformations in column D3 in the full five-story model under the fire scenario with fire load density of 640 MJ/m^2. The calibrated spring stiffnesses are summarized in Table 6 where k_x represents the average restraint stiffness at the top of all upper columns in the Xdirection; k_y represents the average restraint stiffness at the top of all upper columns in the Y direction; k_z represents the average restraint stiffness at the top of all upper columns in the Z direction. k_x is different from k_y since the fire exposure is not symmetrical. In the fire scenario, three frames in the X direction remain at cold temperature while only one frame in the Y direction does; this leads to a greater displacement of the upper stories in Y direction, compared to that in the X direction in the full-building model, e.g., the average displacement in the Y direction is almost 34 times that in the X direction at time = 40 min while the average residual displacement in the Y direction is almost 9.4 times that in the X direction (measured at the top of the second-story columns). When the full-building is simplified into the one-story model, it is assumed that the restraints at the top of second-story columns are represented by springs in the X and Y directions. The difference of the one-story model from the full-building mode in the X and Y displacement at the top of the secondary-story columns will be incorporated into the calibration of the stiffnesses, k_x and k_y, which can explain the great difference between k_x and k_y.

Fig. 15 provides a comparison of the column displacements predicted with the one-story model and the reference full building model. For each translational degree of freedom (X, Y, Z), maximum and residual values of displacements are compared. For the axial displacement, the maximum axial expansion is reported. Residual displacements are read after the temperature in the whole structure has come back to 20 °C. Results indicate that the one-story model with calibrated stiffness can replicate the column behavior in the full building model during and after the fire. Compared to Method 1, this Method 2 can predict both the axial and lateral displacements of the column under consideration.

However, this Method 2 requires a calibration effort to define the stiffnesses of the springs on top of the columns. Besides, the stiffness calibration for the one-story model is performed considering a specific fire scenario (q_f = 640 MJ/m^2) and column of interest (D3). It is verified that the predicted behavior based on these calibrated stiffness remains accurate when considering other fire loads (but keeping the same fire area). Yet, the one-story model with calibrated stiffness only works for the column of interest (D3) or other columns in that story with similar mechanical/thermal boundary conditions and similar initial loads (such as column D4), as shown in Fig. 15b. When comparing displacements at the top of perimeter columns, the one-story model calibrated for an interior column only gives an approximate representation of the full building model. As a result, this modeling technique is efficient for capturing the behavior of one specific column, for which it needs to be calibrated, but is limited for capturing the response of all columns.

5.3. Method 3: Simplified full building model

As discussed in Method 2, the accuracy of the one-story model cannot be guaranteed in predicting the residual deformation of columns which have mechanical/thermal boundary conditions and initial loads different from the column used for calibration. Therefore, a more sophisticated modeling method is introduced.

As fires were assumed on the ground floor, the structural members in the first story and those directly connected to the first story were primarily subject to thermal effects. The upper stories transfer loads to the fire-exposed story through RC frames and provide the boundary restraints to the fire-exposed story by the columns. On account of the high computation time of the full building model due to the modelling of slab using shell elements, Method 3 ignores the floors in the upper-

Table 5
Comparing the numerical residual deformations from the full building model and the isolated column model. Deformations are given for the three translational degrees of freedom at the top of the columns, in mm.

		Two-side fire (F1)		Three-side fire (F2)		Four-side fire (D3)	
		Full	Isolated	Full	Isolated	Full	Isolated
640 MJ/m^2	X	−53.8	−1.5	−34.3	0.1	−10.6	−0.1
	Y	−57.5	−1.5	−57.7	−0.2	−18.3	−0.1
	Z	−4.3	−3.1	−20.6	−8.6	−9.1	−8.9

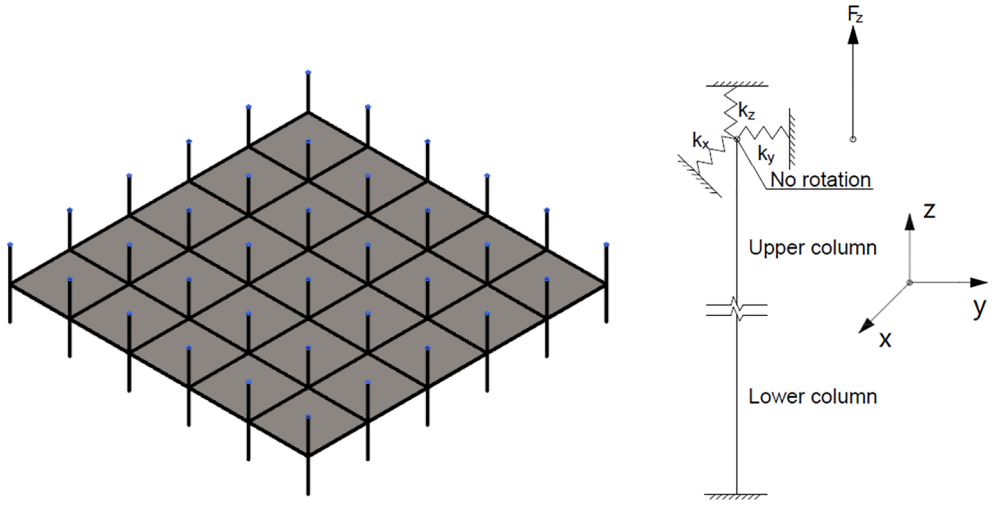

Fig. 14. One-story model.

Table 6
Calibrated spring stiffness of the one-story model.

k_x	k_y	k_z
(kN/m)	(kN/m)	(kN/m)
20 000	550	32 500

stories and keeps the beam-column frames which directly influence the behavior of the fire-exposed story, as shown in Fig. 16. The fire-exposed story and the columns of the second story which are directly connected to the fire-exposed story were modelled in detail using a relatively fine mesh, while the other RC frame members were modelled using relatively coarse mesh without slabs. The coarse frame from the third floor to the roof can still represent the restraint exerted to the fire-exposed story and meanwhile transfers the loads from the upper stories to the first story. This method reduces the computation time noticeably by reducing the number of shell elements in the model. The computation time of the simplified full building model is about 50% of that of the full building model.

Fig. 17 shows the displacement comparison of column D3 obtained from the full building model and the simplified full building model. This method can predict the deformations of any column in the first story, as can be noticed if Fig. 18 is compared with Fig. 9. Besides, it does not require any calibration process for restraint stiffness since it does not include springs.

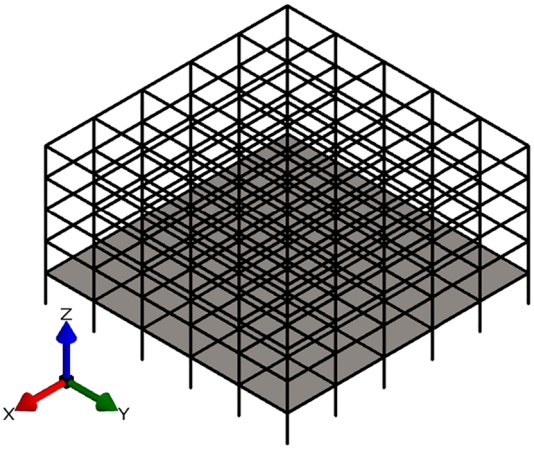

Fig. 16. Simplified full building model.

6. Parametric study of the residual deformations of RC columns

Most previous parametric studies focused on the fire resistance of RC structural components during the fire [49,50], rather than their

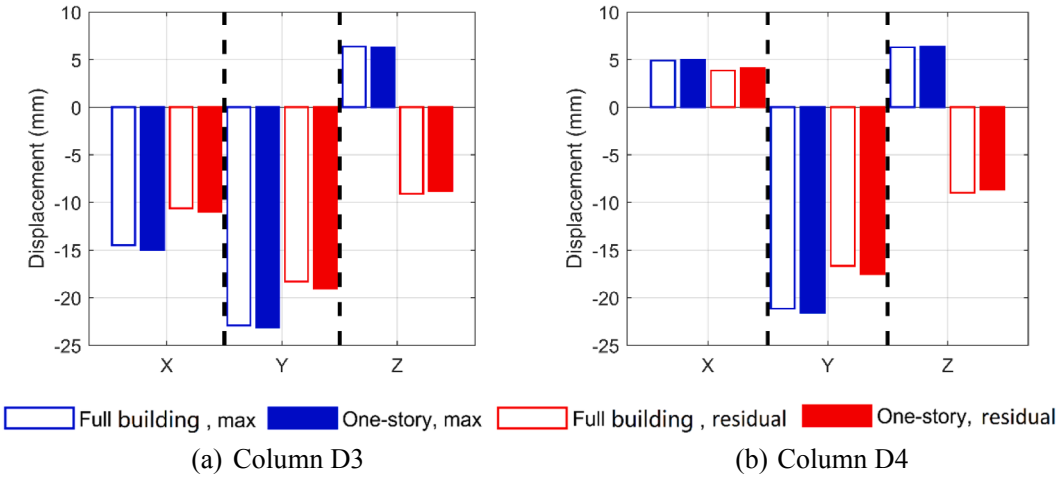

Fig. 15. Comparison of displacements of column D3 and D4 from one-story model and full building model under the fire scenario with $q_f = 640\ MJ/m^2$.

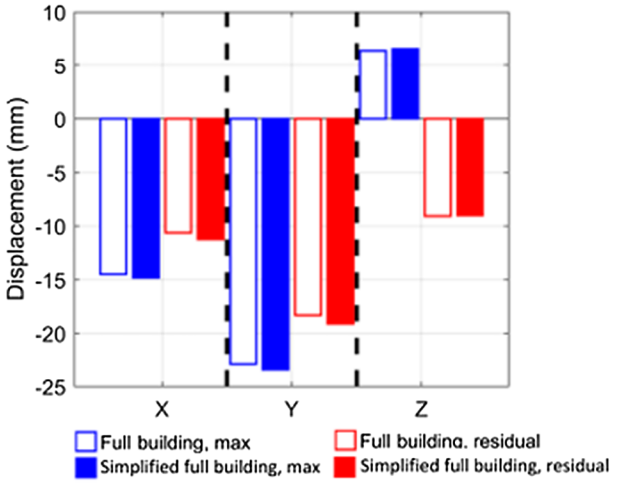

Fig. 17. Comparison of displacements of column D3 from simplified full building model and full building model under fire scenario with q_f = 640 MJ/m^2.

characteristics after fire exposure. A parametric study of the residual deformations of RC columns is presented in this section. This parametric study covers four critical parameters, namely fire load density (q_f), opening factor (O), thermal conductivity of concrete (through coefficient α as previously defined) and applied factored live loads (L, 0.5 times nominal live load). These parameters are chosen to influence the thermo-mechanical problem of the structural response in fire, with effects on the fire development, heat transfer problem and structural behavior. The numerical analysis is conducted using the simplified full building model.

The reference case is characterized by q_f = 320 MJ/m^2, O = 0.035 m$^{1/2}$, α = 0.5 and L = 1.2 kPa, and focusing on column D3. According to clause 3.3.3 of EN 1992-1-2 [25], the thermal conductivity can be chosen between lower and upper limit values. The parameter α (0 ~ 1) allows any intermediate value of concrete thermal conductivity to be taken from the lower and upper limits in EN 1992-1-2 [25]. The other parameters of the reference case are listed in Table 2. The other cases alter one characteristic of the reference analysis to allow for a consistent baseline for discussion. Table 7 summarizes the cases analyzed in the parametric study. Highlighted cells indicate values different from the reference case. In all analyses, parameters not listed in Table 7 are the same as those in Table 2. With respect to the opening factor, the fire is ventilation-controlled for opening factors equal to 0.02 m$^{1/2}$ and 0.035 m$^{1/2}$ (reference case) while it is fuel-controlled for opening factors equal to 0.09 m$^{1/2}$, 0.145 m$^{1/2}$ and 0.2 m$^{1/2}$.

The analyses with fire load density of 800 MJ/m^2 and applied factored live load of 2.4 kPa fail to converge numerically during the cooling phase. These cases correspond to extreme values of the fire intensity or applied mechanical loading. At the end of the simulation, concrete crushes and steel reinforcement yields in the regions with large deformation under fire, such as the column F2 and its surrounding structural members, shown in Fig. 19 where the deformed shape at failure is presented.

According to Fig. 20, as the fire load density increases, the residual deformation at the top of Column D3 increases in both the lateral and

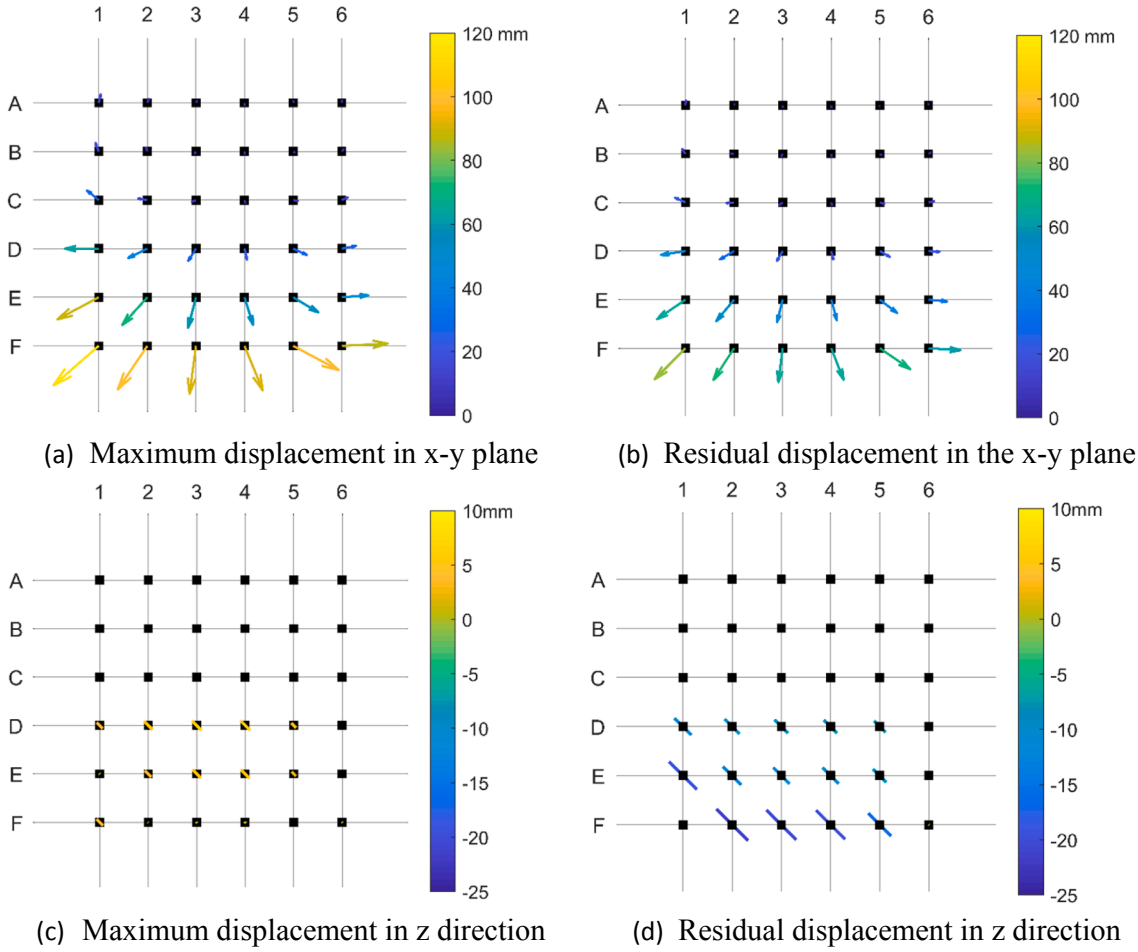

Fig. 18. Color map of maximum and residual column deflections under fire scenario with q_f = 640 MJ/m^2 from simplified full building model.

Table 7
Variation of parameters.

Description	q_f (MJ/m^2)	O (m$^{1/2}$)	α	L (kPa)
Reference	320	0.035	0.5	1.2
Fire load density, q_f	160	0.035	0.5	1.2
	480	0.035	0.5	1.2
	640	0.035	0.5	1.2
	800**	0.035	0.5	1.2
Opening factor, O	320	0.020	0.5	1.2
	320	0.090	0.5	1.2
	320	0.145	0.5	1.2
	320	0.200	0.5	1.2
Parameter for thermal conductivity, α	320	0.2	0	1.2
	320	0.2	0.25	1.2
	320	0.2	0.75	1.2
	320	0.2	1	1.2
Applied factored live load, L	320	0.2	0.5	0
	320	0.2	0.5	0.6
	320	0.2	0.5	1.8
	320	0.2	0.5	2.4**

Note: analysis case with ** means that the structure fails during the fire, the results of which will not be presented in Fig. 20.

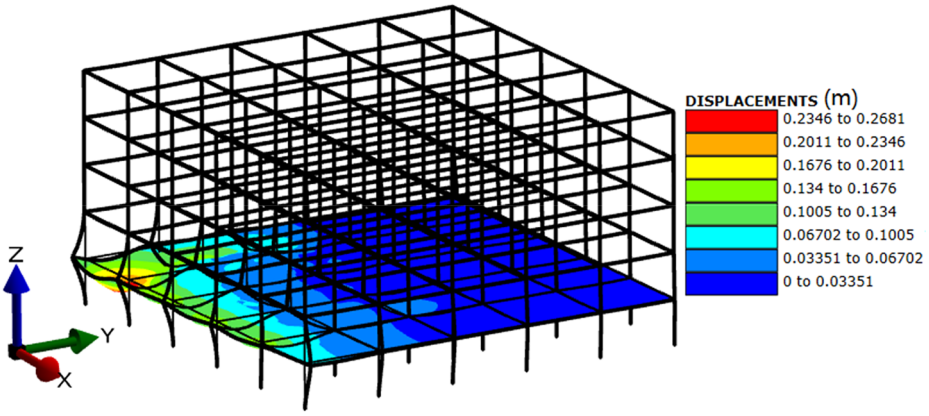

Fig. 19. Residual deformation of the simplified full building model after fire exposure.

axial directions. As the opening factor increases, the fire changes from ventilation-controlled to fuel-controlled. When the fire is still controlled by ventilation, the residual deformation decreases quickly as the opening factor increases. If the opening factor is as low as 0.02 m$^{1/2}$, the gas temperature decreases very slowly during the cooling phase, as shown in Fig. 21. Due to the high thermal inertia of concrete, the maximum temperature in the inside of a section is reached long after the onset of cooling, which is particularly true for the scenario with a slow cooling phase. Therefore, the structural members experience more deformations during the cooling phase and thus have large residual deformations after the fire. When the fire becomes fuel-controlled, the opening factor, which is mainly related to ventilation, does not influence the residual deformation of the columns significantly. According to Fig. 20c, the thermal conductivity of concrete has no significant influence. Live load is also not a critical parameter, as shown in Fig. 20d, due to the relatively high dead loads from the building self-weight. However, regarding live load, the limited influence is only true up to a certain point; beyond this point, the loading becomes so important that the structure fails during the nominal fire event.

7. Conclusion

This paper focuses on the numerical modeling of the effect of fire on a code-designed five-story building with reinforced concrete frame structure. The emphasis is on the residual (post-fire) response after complete burnout, notably the residual deformations of the concrete columns which are the key structural members in assessing the possibility for rehabilitation.

Different computational models are investigated to capture the fire behavior of the columns, ranging from isolated column models with beam and spring finite elements to the full building model with beam and shell finite elements. Results show that the fire causes considerable residual deformations in axial and lateral directions, in addition to significant decrease of the load-bearing capacity. Lateral residual deformations are mainly caused by thermal expansion and contraction of the horizontal structural members (beams and slabs) which generate permanent strains in the structure. The isolated column model fails to capture this effect, resulting in an inaccurate estimation of the residual deformations in the columns after the fire. Two intermediate modeling approaches (one-story model and simplified full building model) are

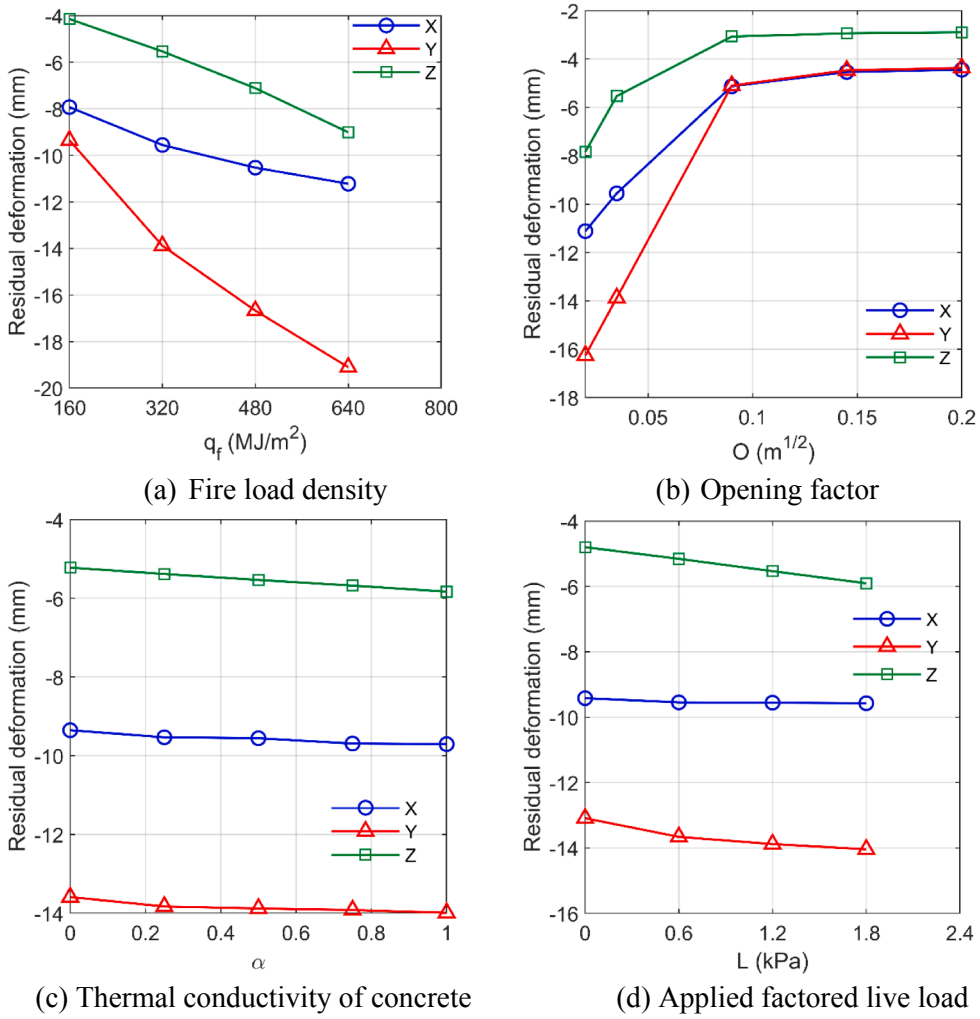

Fig. 20. Parametric variation of the residual deformation along X, Y and Z at the top of column D3.

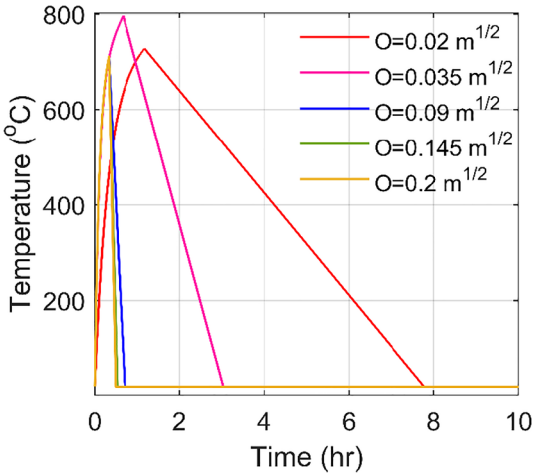

Fig. 21. Parametric temperature-time curves for different opening factors.

described to incorporate the effect of the thermal expansion-contraction of the surrounding beams and slabs on the column with reasonable computational efficiency and accuracy.

A parametric study of the residual deformations of the columns highlighted the effects of different design parameters and fire scenarios on the magnitude of residual deformations of the columns after fire exposure. Four critical parameters were investigated, namely fire load density, opening factor, thermal conductivity of concrete and live loads. Compared to the thermal conductivity of concrete and live loads, fire load density and opening factors significantly influence the residual deformations. The residual deformation of the columns increases with the increase of fire load density and decreases with the increase of the opening factor.

As a result, this research improves the understanding and provides recommendations for numerical modeling of the effect of fire on the residual capacity and deformations in RC structures. Notably, it highlights the importance of structural system level effects, i.e. thermally induced deformations and forces in structural assemblies, on the damage caused by a fire in a building. This corroborates previous studies on the effects of restraint forces in concrete structures exposed to fire [51]. In future research, additional fire scenarios should be considered to analyze the effect of fire compartment area and fire spread on the residual damage. One limitation of the study is that spalling is not included in the model. Further works will also conduct additional sensitivity analyses for the RC building response considering parameters related to structural design. The goal is eventually to construct probabilistic fragility functions for the entire building [52], considering different design alternatives, which can then be used for assessing the fire resilience of RC buildings and infrastructure.

Declaration of Competing Interest

The authors declare that they have no known competing financial interests or personal relationships that could have appeared to influence the work reported in this paper.

Appendix A. Supplementary material

Supplementary data to this article can be found online at https://doi.org/10.1016/j.engstruct.2019.109853.

References

[1] Nene RL, Kavle PS. Rehabilitation of a fire damaged structure. ACI Spec Publ 1991;128. https://doi.org/10.14359/3469.
[2] Molkens T, Van Coile R, Gernay T. Assessment of damage and residual load bearing capacity of a concrete slab after fire: Applied reliability-based methodology. Eng Struct 2017;150:969–85. https://doi.org/10.1016/j.engstruct.2017.07.078.
[3] Beitel J, Commerce UD, Iwankiw N. Analysis of needs and existing capabilities for full-scale fire resistance testing. CreateSpace Independent Publishing Platform 2008.
[4] Wu B, Li Y-H, Chen S-L. Effect of heating and cooling on axially restrained RC columns with special-shaped cross section. Fire Technol 2009;46:231. https://doi.org/10.1007/s10694-009-0091-y.
[5] Kevin AM, Yahya CK. Out-of-plane behavior and stability of five planar reinforced concrete bearing wall specimens under fire. Struct J n.d.;112. doi:10.14359/51687908.
[6] Wu B, Xu Y. Behavior of axially-and-rotationally restrained concrete columns with '+'-shaped cross section and subjected to fire. Fire Saf J 2009;44:212–8. https://doi.org/10.1016/j.firesaf.2008.07.003.
[7] Bernhart D. The effect of support conditions on the fire resistance of a reinforced concrete beam. University of Canterbury; 2004.
[8] Ali F, Nadjai A, Silcock G, Abu-Tair A. Outcomes of a major research on fire resistance of concrete columns. Fire Saf J 2004;39:433–45. https://doi.org/10.1016/j.firesaf.2004.02.004.
[9] Dwaikat MB, Kodur VKR. A numerical approach for modeling the fire induced restraint effects in reinforced concrete beams. Fire Saf J 2008;43:291–307. https://doi.org/10.1016/j.firesaf.2007.08.003.
[10] Lie T, Lin T. Influence of restraint on fire performance of reinforced concrete columns. Fire Saf Sci 1986;1:291–300. https://doi.org/10.3801/IAFSS.FSS.1-291.
[11] Abu AK, Burgess IW, Plank RJ. Effects of edge support and reinforcement ratios in slab panel failure in fire. In: Tan KH, Kodur VKR, Tan TH, editors. 5th Int. Conf. SIF, Singapore: SiF 2008 Organising Committee; 2004. p. 380–91.
[12] Wu B, Liu J, Chen X. Numerical analysis of lateral displacement of beam-column joints in concrete frame structures subjected to fire. Adv Struct Eng 2017;21:1495–509. https://doi.org/10.1177/1369433217749767.
[13] Gernay T. Fire resistance and burnout resistance of reinforced concrete columns. Fire Saf J 2019;104:67–78. https://doi.org/10.1016/j.firesaf.2019.01.007.
[14] Angus Law MG. Load induced thermal strains, implications for structural behaviour. In: Tan KH, Kodur VKR, Tan TH, editors. Fifth Int. Conf. Struct. Fire, Nanyang Technological University, Singapore: SiF 2008 Organising Committee; 2008. p. 488–96.
[15] Gernay T. Effect of transient creep strain model on the behavior of concrete columns subjected to heating and cooling. Fire Technol 2012;48:313–29.
[16] Al Hamd RKS, Gillie M, Warren H, Torelli G, Stratford T, Wang Y. The effect of load-induced thermal strain on flat slab behaviour at elevated temperatures. Fire Saf J 2018;97:12–8. https://doi.org/10.1016/j.firesaf.2018.02.004.
[17] Franssen J-M, Gernay T. Modeling structures in fire with SAFIR®: theoretical background and capabilities. J Struct Fire Eng 2017;8:300–23. https://doi.org/10.1108/JSFE-07-2016-0010.
[18] Al Mamun A, Saatcioglu M. Seismic fragility curves for reinforced concrete frame buildings in Canada designed after 1985. Can J Civ Eng 2017;44:558–68. https://doi.org/10.1139/cjce-2016-0388.
[19] NBCC 2010. National building code of Canada. National Research Council of Canada. Ottawa, Canada; 2010.
[20] CSA A23.3-04. Design of concrete structures. Canadian Standards Association. Mississauga, Ont., Canada; 2004.
[21] IBC 2018. International building code. International Code Council. Country Club Hills, IL, USA; 2018.
[22] BS EN1991-1-2. Eurocode 1: Actions on structures - Part 1-2: General actions - Actions on structures exposed to fire. European Standard; 2002.
[23] Gernay T, Millard A, Franssen J-M. A multiaxial constitutive model for concrete in the fire situation: Theoretical formulation. Int J Solids Struct 2013;50:3659–73. https://doi.org/10.1016/j.ijsolstr.2013.07.013.
[24] Franssen J-M. Thermal elongation of concrete during heating up to 700°C and cooling; Stress-strain relationship of Tempcore steel after heating up to 650°C and cooling. Liège, Belgique: Univ. de Liège; 1993. doi:http://hdl.handle.net/2268/531.
[25] BS EN 1992-1-2. Eurocode 2. Design of concrete structures - Part 1-2: General rules. Structural fire design. European Standard; 2004.
[26] BS EN 1993-1-2. Eurocode 3. Design of steel structures - Part 1-2: General rules - Structural fire design. European Standard; 2005.
[27] Izumo JHS, Maeakawa K, Okamura H. An analytical model for RC panels subjected to in-plane stresses 1st ed. In: Hsu TCC, Mau ST, editors. Concr. Shear EarthqCRC Press; 1992. p. 206–15.
[28] Collins MP, Mitchell D. Prestressed concrete basics. Ottawa, Ont.: Canadian Prestressed; 1987.
[29] Vecchio F, Collins MP. The response of reinforced concrete to in-plane shear and normal stresses. Department of Civil Engineering, University of Toronto; 1982.
[30] Martinez J, Jeffers AE. Elevate-temperature tension stiffening model for reinforced concrete structures under fire. In: Nadjai A, Ali F, Franssen J-M, Vassart O, editors. 10th int. conf. struct. Fire, Ulster University. Belfast, UK: Ulster University; 2018. p. 463–70.
[31] Talamona D, Franssen J-M. A quadrangular shell finite element for concrete and steel structures subjected to fire. J Fire Prot Eng 2005;15:237–64. https://doi.org/10.1177/1042391505052769.
[32] Vassart O, Bailey CG, Hawes M, Nadjai A, Simms WI, Zhao B, et al. Large-scale fire test of unprotected cellular beam acting in membrane action. Proc Inst Civ Eng - Struct Build 2012;165:327–34. https://doi.org/10.1680/stbu.11.00019.
[33] Gernay T, Franssen J-M. A plastic-damage model for concrete in fire: Applications in structural fire engineering. Fire Saf J 2015;71:268–78. https://doi.org/10.1016/j.firesaf.2014.11.028.
[34] Lim L, Wade C. Experimental fire tests of two-way concrete slabs. Christchurch, New Zealand: University of Canterbury; 2002. doi:http://hdl.handle.net/10092/8476.
[35] Bernd K, Kaspar W. Question of tension softening versus tension stiffening in plain and reinforced concrete. J Eng Mech 2008;134:804–8. https://doi.org/10.1061/(ASCE)0733-9399(2008) 134:9(804).
[36] Anderberg Y, Thelandersson S. Stress and deformation characteristics of concrete at high temperatures. 2. Experimental investigation and material behaviour model. vol. Bulletin 5. Lund Institute of Technology 1976.
[37] Anderberg Y. Fire-exposed hyperstatic concrete structures: An experimental and theoretical study. Spec Publ n.d.;55. doi:10.14359/6623.
[38] Gernay T, Franssen JM. A formulation of the Eurocode 2 concrete model at elevated temperature that includes an explicit term for transient creep. Fire Saf J 2012;51:1–9. https://doi.org/10.1016/j.firesaf.2012.02.001.
[39] Schneider U. Properties of materials at high temperature: Concrete. University of Kassel; 1985.
[40] BS EN 1994-1-2. Eurocode 4 - Design of composite steel and concrete structures - Part 1-2: General rules - Structural fire design. European Standard; 2005.
[41] Smith CI, Kirby BR, Lapwood DG, Cole KJ, Cunningham AP, Preston RR. The re-instatement of fire damaged steel framed structures. Fire Saf J 1981;4:21–62. https://doi.org/10.1016/0379-7112(81)90004-7.
[42] Kirby BR, Thomson G. LDG. The reinstatement of fire damaged steel and iron framed structures. B.S.C., Swinden Laboratories; 1986.
[43] Outinen J, Mäkeläinen P. Mechanical properties of structural steel at elevated temperatures and after cooling down. Fire Mater 2004;28:237–51. https://doi.org/10.1002/fam.849.
[44] Qiang X, Bijlaard FSK, Kolstein H. Post-fire mechanical properties of high strength structural steels S460 and S690. Eng Struct 2012;35:1–10. https://doi.org/10.1016/j.engstruct.2011.11.005.
[45] Gernay T. A multiaxial constitutive model for concrete in the fire situation including transient creep and cooling down phases. University of Liege; 2012.
[46] Ni S, Birely AC. Post-fire earthquake resistance of reinforced concrete structural walls. In: 11th Can Conf Earthq Eng; 2015. p. 1–9.
[47] Ni S, Birely AC. Post-fire seismic behavior of reinforced concrete structural walls. Eng Struct 2018;168:163–78. https://doi.org/10.1016/j.engstruct.2018.04.018.
[48] Su LF. Fire resistance of high strength concrete columns under axial restraint. Nanyang: Technological University; 2008.
[49] Lie TT. Fire resistance of reinforced concrete columns: A parametric study. J Fire Prot Eng 1989;1:121–9. https://doi.org/10.1177/104239158900100402.
[50] Xu Y, Wu B. Fire resistance of reinforced concrete columns with L-, T-, and +-shaped cross-sections. Fire Saf J 2009;44:869–80. https://doi.org/10.1016/j.firesaf.2009.04.002.
[51] Annerel E, Taerwe L, Merci B, Jansen D, Bamonte P, Felicetti R. Thermo-mechanical analysis of an underground car park structure exposed to fire. Fire Saf J 2013;57:96–106. https://doi.org/10.1016/j.firesaf.2012.07.006.
[52] Gernay T, Elhami Khorasani N, Garlock M. Fire fragility curves for steel buildings in a community context: A methodology. Eng Struct 2016;113:259–76. https://doi.org/10.1016/j.engstruct.2016.01.043.